

Wall-Street: Smart Surface-Enabled 5G mmWave for Roadside Networking

Kun Woo Cho¹, Prasanthi Maddala², Ivan Seskar², Kyle Jamieson¹
Princeton University¹, Rutgers University²

Abstract

5G mmWave roadside networks promise high-speed wireless connectivity, but face significant challenges in maintaining reliable connections for users moving at high speed. Frequent handovers, complex beam alignment, and signal attenuation due to obstacles like car bodies lead to service interruptions and degraded performance. We present **Wall-Street**, a smart surface installed on vehicles to enhance 5G mmWave connectivity for users inside. Wall-Street improves mobility management by (1) steering outdoor mmWave signals into the vehicle, ensuring coverage for all users; (2) enabling simultaneous serving cell data transfer and candidate handover cell measurement, allowing seamless handovers without service interruption; and (3) combining beams from source and target cells during a handover to increase reliability. Through its flexible and diverse signal manipulation capabilities, Wall-Street provides uninterrupted high-speed connectivity for latency-sensitive applications in challenging mobile environments. We have implemented and integrated Wall-Street in the COSMOS testbed and evaluated its real-time performance with four gNBs and a mobile client inside a surface-enabled vehicle, driving on a nearby road. Wall-Street achieves a 2.5-3.4× TCP throughput improvement and a 0.4-0.8× reduction in delay over a baseline 5G Standalone handover protocol.

1 Introduction

Fifth generation (5G) wireless networks have recently introduced millimeter wave (mmWave) technology in the FR2 frequency band to meet the ever-increasing demand for high-speed, low-latency service [3]. With its abundant spectrum resources and wide bandwidth, mmWave communication has the potential to deliver multi-gigabit data rates, enabling a plethora of innovative applications such as virtual reality, augmented reality, and seamless streaming of ultra high-definition video [23]. However, the unique characteristics of mmWave signals pose significant challenges in maintaining reliable connectivity, particularly in high mobility scenarios [24].

One of the primary obstacles in mmWave communication is its susceptibility to blockage [17] and high path loss: due to its short wavelengths and limited diffraction capability, mmWave signals are easily obstructed by common obstacles such as buildings, foliage, and even the human body [5, 13, 28, 33]. This necessitates a dense deployment of small cells to ensure adequate coverage, resulting in frequent handovers as users move between cells. Indeed, mmWave 5G New Radio (NR)

experiences a handover (HO) significantly more often than LTE or low band 5G NR, [11, 20]. Moreover, the handover process in mmWave networks complicates the already-complex low band handover [7, 31], involving additionally precise alignment of the narrow beam between user equipment (UE) and base station (BS) [28], and requiring the UE to continuously measure the signal strength of neighboring cells and report it to the serving BS, which then decides when and to which cell to handover the UE.

High delays associated with mmWave handovers have significant impacts throughout the entire protocol stack, from the physical layer to the application layer, degrading quality of service (QoS) for end users, especially for latency-sensitive applications [11, 19]. To prepare a handover, the UE periodically suspends data communication with the serving BS to perform neighboring cell measurements. This process requires users to engage in an exhaustive search for the strongest signal from neighboring BSs, resulting in bufferbloat and slow growth of the congestion window [18]. Furthermore, the handover decision relies on these measurement reports, which may be outdated or lost due to the rapidly changing channel conditions and potential disconnections. This can trigger unnecessary handovers and lead to transport protocol connection timeouts, impacting overall network performance.

This paper presents the design and implementation of Wall-Street, a smart surface that transforms 5G mmWave connectivity, specifically for vehicular use scenarios. In such high-mobility scenarios, we install **Wall-Street** on vehicles to improve connectivity for users inside. Wall-Street leverages the concept of a programmable mmWave smart surface [6] to manipulate and steer mmWave signals, enabling seamless coverage and reliable communication for vehicle users. By strategically deploying Wall-Street on the exterior of vehicles, we aim to mitigate the impact of signal blockage and attenuation caused by the vehicle body, ensuring that mmWave signals can effectively penetrate and reach users inside the vehicle. Moreover, the handover (HO) process in mmWave networks consumes at least twice the energy per unit distance, compared to low-band HOs [11]. Wall-Street reduces UE HO energy consumption by letting the surface perform neighboring cell signal strength measurements. Three key innovations of Wall-Street (Fig. 1) enable seamless vehicular-speed mmWave networking:

1. In-vehicle mmWave coverage. Wall-Street efficiently steers outdoor mmWave signals into a vehicle, providing consistent coverage for all users within (Fig. 1(a)) and eliminates

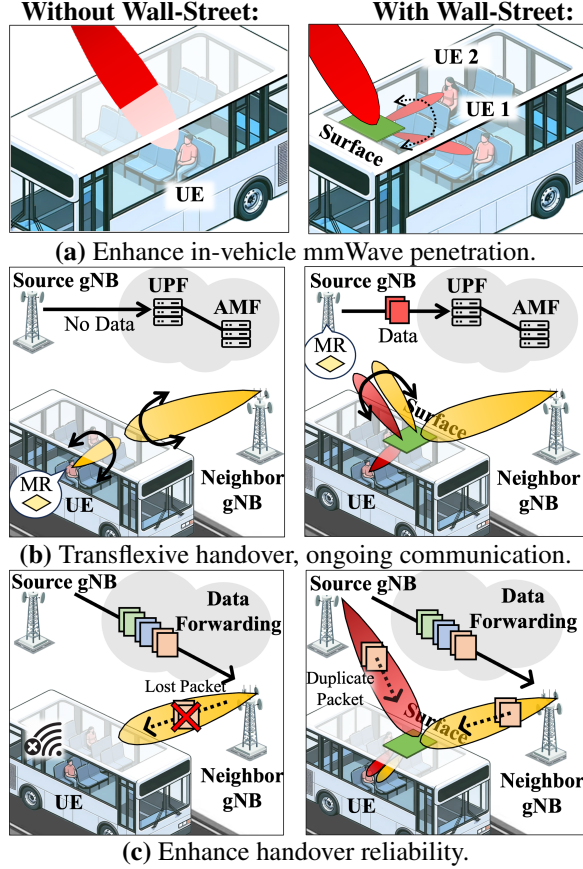


Figure 1— Wall-Street’s design innovations electronically split, shape, and steer mmWave transmissions in real time to enable seamless roadside 5G New Radio networks.

the need for individual users to each undergo separate handover processes.

2. Seamless handover with concurrent communication. Innovating beyond previous programmable mmWave surfaces [6], Wall-Street is the first design that can simultaneously reflect, refract, and split the mmWave beam at arbitrary angles, with low signal strength loss. Leveraging this *transflexive* property, the Wall-Street system enables simultaneous data exchange and neighboring cell measurement by reflecting the synchronization signal bursts from neighboring cells directly to the serving BS while refracting the data communication link between the serving BS and UE, as shown in Fig. 1(b) (right). This innovative dual functionality (simultaneous transmissive and reflective beam steering) allows for seamless handovers without service interruption, as the UE can continue to communicate with the serving base station (gNB) while the gNB performs the necessary measurements.

3. Make-before-break handover. At the moment of handover, when signal strength is typically weakest, Wall-Street facilitates the transmission of duplicate data packets from both the source and the new serving cell by combining two beams and steering them directly to the UE. This dual-beam combination significantly boosts the reliability during han-

dover execution. By adjusting the power of the respective links, Wall-Street ensures an uninterrupted flow of data, minimizing packet loss and retransmissions.

We have designed and implemented Wall-Street hardware and integrated it into the COSMOS testbed [25], incorporating new PHY features on its USRP-based mmWave gNBs and UE. This integration enables real-time handover experiments in environments that match the scenarios depicted in Fig. 1. §4 provides a detailed description of our implementation of the Wall-Street-integrated COSMOS testbed. We mount Wall-Street on the rear door of an SUV vehicle and deploy a mobile UE on the rear seat, with four gNBs placed on the first floor of a lab facing the road. We also implemented the 5G Standalone handover protocol and used it as a performance benchmark for our evaluation. To evaluate TCP end-to-end performance, we use a state-of-the-art mmWave ns-3 simulator [18] with our own modifications, in SA mode. The simulation is trace-driven, fed with PHY traces collected from real-time experiments. Our results demonstrate a 2.5-3.4× improvement in TCP throughput and a 0.4-0.8× reduction in delay compared to the baseline 5G Standalone handover protocol. Also, we observe more than a 0.5× reduction in unnecessary handover events. We further evaluate the impact of vehicle speed and the performance improvement at different handover stages. Microbenchmarks investigate Wall-Street’s in-vehicle coverage improvement, beam tracking, and multi-link capabilities, its far-field and near-field beam patterns. These benchmarks provide insights into the enhanced performance and new capabilities offered by Wall-Street.

2 Primer: 5G Mobility Management

We introduce the state of the art in 5G New Radio (NR) Standalone (SA) beam acquisition and tracking (§2.1), followed by 5G SA handover (§2.2), standardized in 3GPP 38.802 [1]. In contrast to Non-Standalone (NSA) handover, SA handover obviates the need to involve legacy 4G infrastructure in the handover [11], making it the cutting edge in 5G.

2.1 Initial Attachment and Tracking

Initial attachment of the UE to the gNB begins via a coarse spatial *beam sweep* of beam directions at both gNB and UE, which 3GPP calls *Procedure 1* (P-1). During the beam sweep in the first 5 ms of each period, the gNB transmits a *synchronization signal burst* comprised of 64 *Synchronization Signal Blocks* (SSBs). The gNB groups M SSBs together, transmitting all of them in the same direction before moving on to the next direction, as shown in Fig. 2(a). This transmission happens periodically, every 20 ms in the mmWave FR2 band by default. The UE scans all its receive directions in the corresponding time it takes the gNB to send M SSBs, so rendezvous is possible. The UE sends its measurement of

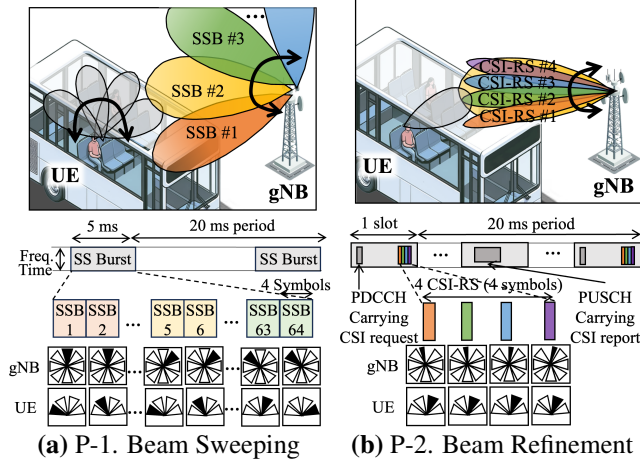


Figure 2— 5G SA beam acquisition and beam tracking.

the SSB's signal strength in a *measurement report* (MR) back the gNB, which confirms the transmit beam, thus initially aligning the transmit and receive beams. Finally, the UE and gNB exchange uplink and downlink data through the selected beam patterns.

After initial attachment and during ongoing communication, the beam directions between the gNB and UE need to be refined and tracked in the face of UE mobility, a process 3GPP calls *Procedure 2* (P-2). The gNB uses transmit beams narrower than those used in P-1, and centered on the beam direction chosen during P-1. During P-2, the gNB scans different fine-grained directions on different channel state information reference signal (CSI-RS) resource blocks, while the receive beam direction of the UE is fixed. The UE sends a CSI-RS to the gNB, which chooses the optimal fine-grained transmit beam direction. To track and refine UE beam directions, *Procedure 3* (P-3) uses CSI-RS combined with a static transmit beam and different UE receive beams.

2.2 5G SA Handover

Today's state of the art 5G Standalone (SA) handover is called *Xn handover*, named after the *Xn interface*, the API interface between two gNBs. The Xn interface allows gNBs to communicate and exchange information related to the handover process. The handover procedure begins with the UE periodically generating and sending a *measurement report* containing the neighboring gNB's identifier, and the corresponding signal strength to the *source gNB* (with which the UE is currently communicating), which then takes the decision to start the handover procedure to the best *target gNB*. Finally, the target gNB completes the handover procedure. SA Xn handover is divided into three main phases: *Preparation*, *Execution*, and *Completion*, as outlined in Fig. 3.

(1) Preparation phase. 5G SA relies on client-side feedback to trigger handovers. The source cell requests the UE to stop the ongoing transmission and perform P-1 measurements to

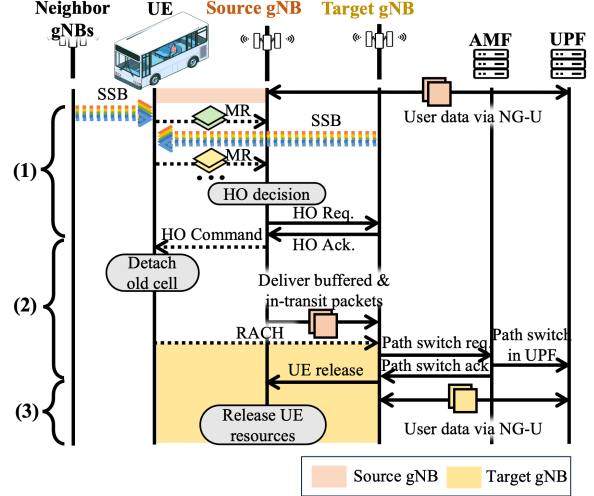


Figure 3— 5G SA Xn handover: (1) Preparation phase; (2) Execution phase; (3) Completion phase. Data communication is denoted with orange and yellow rectangles.

measure the received power of the reference signal (*Reference Signal Received Power*, or RSRP) for each neighboring cell. A common trigger for 5G handover is *event A3* [7, 31], which specifies that the signal strength of the neighboring cell is higher than that of the current serving cell by a certain hysteresis threshold, *i.e.*:

$$M_n - H > M_s \quad (1)$$

where M_n and M_s are the respective RSRPs of the neighboring and source cells, and H is a hysteresis parameter. To avoid ping-pong handover caused by signal fluctuations, a time-to-trigger (TTT) is used as the time hysteresis: the HO is triggered when Eq. (1) holds true for the TTT duration.

(2) Execution phase. The source gNB decides to initiate a handover and sends a *handover request* (HO Req) —Fig. 3, Step (2)—to the chosen target gNB over the Xn interface. The target BS responds with an acknowledgement, providing the necessary resources for the UE. Upon receiving the acknowledgement, the source BS sends a *Handover Command* (HO Command) to the UE, instructing it to detach from the source gNB and synchronize with the target gNB using the *Random Access Channel* (RACH) procedure. The source gNB starts buffering data coming from the 5G Core (5GC) *user plane function* (UPF) and forwards it to the target gNB.

(3) Completion phase. The target gNB sends a Path Switch request message to the 5GC, informing it about the handover and requesting an update of the UE's downlink path. The 5GC updates the UE's downlink path and sends a Path Switch Request Acknowledge message to the target gNB. The target gNB sends a UE Context Release message to the source gNB over the Xn interface, indicating that the handover is complete. The source gNB then releases the UE's context.

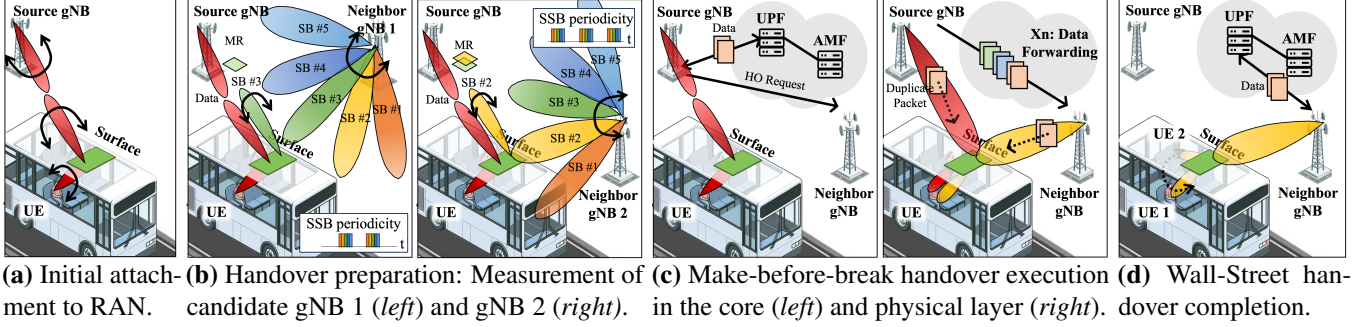


Figure 4— Wall-Street design overview: (a) Initial UE-RAN attachment (§3.1.1); (b) preparation using transfective surface power measurement to multiple cells (§3.2.1); (c) beam combining to enable make-before-break dual-cell connectivity (§3.2.2); (d) handover completion (§3.2.3).

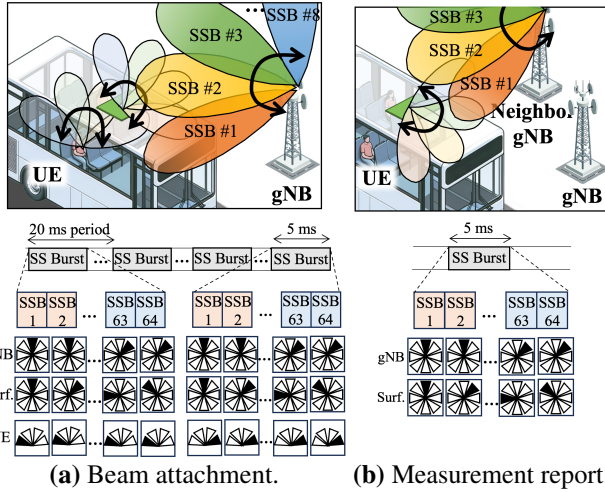


Figure 5— Wall-Street process: beam attachment and measurement report process corresponding to Fig. 4(a) and Fig. 4(b), respectively. Beam attachment and measurement report require four SS bursts and one SS burst of five-millisecond duration.

3 Design

This section presents the design of Wall-Street, which is summarized graphically in Fig. 4. Section 3.1 describes the normal operations of UE attachment and tracking. Section 3.2 walks the reader through Wall-Street’s handover.

3.1 Attachment and Tracking

Wall-Street’s normal operation requires UEs to attach to the RAN, and the RAN to track their movement. We detail how the UE initially attaches to the gNB and determines an optimal set of beam patterns via SSB measurements (§3.1.1), and how the gNB tracks the Wall-Street UE in motion (§3.1.2)

3.1.1 Initial Attachment

Similar to 5G NR, Wall-Street attachment adapt to function under practical timescales with a surface. First, a UE needs to

be able to attach to the gNB of the RAN through Wall-Street. This process, shown at a high level in Fig. 4(a), begins with a SSB beam sweep at each of the gNB, Wall-Street, and UE, as detailed in Fig. 5(a). During a single SS burst, the UE fixes its beam angle while both Wall-Street and the gNB spatially sweep their beams. With each UE angle, the UE makes an SS Burst power measurement, each with a different beam pattern—which it feeds back to the gNB via a *beam report*. Practically, four SS bursts are needed (corresponding to each of four different UE receive beam patterns) for this initial paging search (80 ms).

3.1.2 Mobile User Tracking

Wall-Street adopts and leverages 3GPP P-2 and P-3 functionality for gNB- and UE-side beam tracking, respectively (§2.1). In addition, Wall-Street devises the following surface-driven *path diversity tracking* algorithm that fuses measurement reports acquired from handover preparation, to bolster the reliability of the sensitive mmWave tracking process. Instead of relying on client-side report, the source gNB directly generates measurement reports by triggering Wall-Street to reflect neighboring gNB’s SSBs and receiving reflected SSBs, as shown in Fig. 4(b) and Fig. 5(b). We will further describe this procedure in §3.2.1.

After beam acquisition and measurement report at a given time t , the source gNB has knowledge of 1) θ_s , its own downlink beam angle, 2) θ_r , the angle by which Wall-Street deflects the UE’s uplink transmission, 3) θ_n , the (non-Snellian) angle by which Wall-Street reflects a neighboring gNB’s downlink transmission, relative to the hypothetical Snellian reflection angle, because the source gNB has control over the surface, and 4) θ_n , the neighboring gNB’s downlink beam angle via mapping a SSB Beam ID from reflected SSBs, as diagrammed in Fig. 6(a). Importantly, we observe that every measurement report period of time (160 ms) a neighboring gNB sends an SSB burst, updating the source cell’s knowledge of parameters θ_r and θ_n (which we define θ'_r and θ'_n respectively), as shown in Fig. 6(b).

Now our objective is to calculate 1) $\Delta\theta_s$, a source gNB

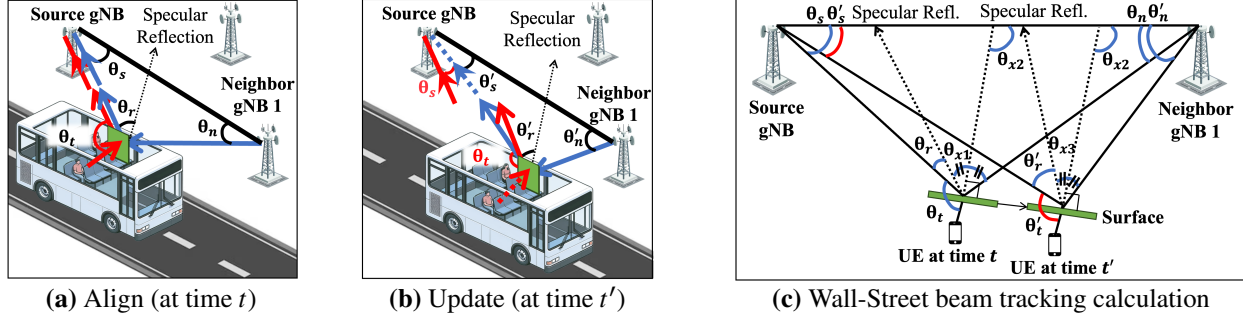


Figure 6— Beam tracking: Wall-Street’s surface-enabled beam tracking leverages neighboring gNBs to add path diversity.

beam angle update, and 2) $\Delta\theta_r$, a surface transmissive beam steering angle update, both for the time step $t' - t$. For this, we first calculate the (hypothetical) Snellian specular reflection angle of the SS burst from the neighboring gNB 1 $\theta_{x1} = (180^\circ - (\theta_s + \theta_n) - \theta_r)/2$ as illustrated in Fig. 6(c). Then, we calculate the normal direction of the surface with respect to the source and neighbor gNBs $\theta_{x2} = \pi - (\theta_{n1} + \theta_{x1})$. In 160 ms, a vehicle moving at 40 mph travels less than three meters, so the surface orientation remains approximately the same. Hence we calculate the specular angle of SSB signals at t' as $\theta_{x3} = 180^\circ - \theta'_n + \theta_{x2}$. Finally, the source cell angle update is $\Delta\theta_s = \pi - (2\theta_{x3} + \theta_{r2}) - \theta_{n2} - \theta_{s1}$, and the surface transmissive beam deflection angle update is $\Delta\theta_t = (\theta_{x3} + \theta_{r2}) - (\theta_{x1} + \theta_{r1})$.

3.2 Cell-to-Cell Handover

This section describes Wall-Street’s cell to cell handover, the first step of which is preparation, which also leverages Wall-Street’s transmissive capability to take reflective measurements of neighboring cells while communication through the surface continues uninterrupted (§3.2.1). Section 3.2.2 presents our make-before-break handover, made possible by the combining of two beams: one from the source cell and another from the target cell. Section 3.2.3 concludes with a description of handover completion, releasing the source cell. Figure 7 summarizes the overall sequence of events, which we refer to throughout this section.

3.2.1 Handover Preparation

We begin at the network layer, which is implemented inside the 5G core. Before handover, the source and neighbor gNB already have an active Xn (§2.2) connection, and the UE is in the RRC *connected* mode, sending and receiving data to and from the source gNB. Periodically, the source gNB sends a control signal via the robust, sub-6 GHz FR 1 band to Wall-Street, triggering the preparation at the physical layer that we describe next, a process that measures the RSRP of reflected SSBs. To avoid collisions, the gNBs separate their respective SSBs in frequency and time across different gNBs, allowing the source gNB to listen to other cells’ SSBs while simultaneously exchanging data with the UE.

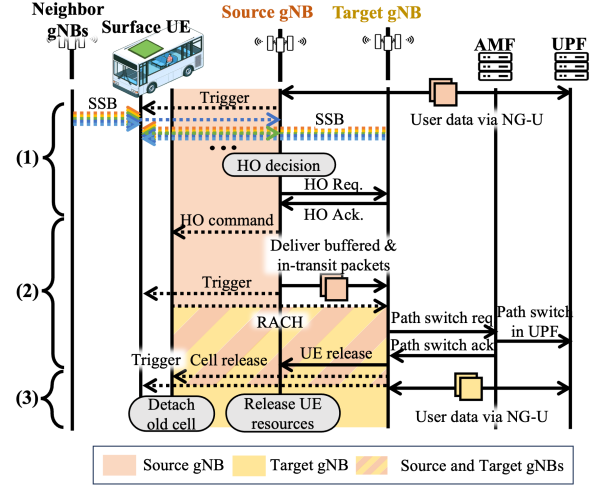


Figure 7— Wall-Street’s handover timeline: 1) Preparation, 2) Execution, and 3) Completion phases are indicated.

Handover preparation at the PHY: Upon receiving a beam measurement trigger from the source gNB, Wall-Street alternates between bi-directional beam combination for uplink data (refracting signals from the UE and reflecting signals from neighboring gNBs) and bi-directional beam splitting for downlink data (refracting signals to the UE and reflecting signals from neighboring gNBs). During this process, the UE’s beam angle, the source gNB’s beam angle, and Wall-Street’s reflective beam angle remain the same, and only Wall-Street’s reflective beam and the neighboring gNB’s beam sweep in one SS Burst, as depicted in Fig. 5(b).

As Wall-Street allows flexibility in the proportion of power allocated to its refractive and reflective beams on the uplink, now the issue arises of how to compute a power split that optimizes end-to-end performance. To this end, we take a max-min approach where our figure of merit is the maximization of the signal strength of the transmissive link between source gNB and UE (to maximize spectral efficiency on the link in use), subject to the maintainance of a minimum signal strength for the reflective link from source to target gNB (to simply keep the candidate handover link up).

Power allocation algorithm: Initially, we allocate maximum power to the reflective link. For each measurement iteration,

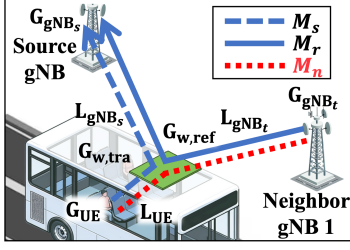


Figure 8— Measurement power translation: Inferring 3GPP-standard measurement report power readings based on Wall-Street’s reflective measurement report readings.

the source gNB gradually increases Wall-Street’s gain while simultaneously monitoring the RSRP of the received SSBs. The algorithm continues to increase the transmission gain until the point at which the SSB is no longer detected, indicating that the optimal power ratio has been reached. The algorithm then slightly reduces the transmission gain, setting it just below the point to maintain the optimal power ratio. By following this procedure, Wall-Street effectively balances the power distribution between the refractive and reflective links (see Fig. 19 in §5.3).

RSRP inference for HO decision. The RSRP of the neighbor gNB’s measurement report as received by the source gNB, M_r , is distinct from M_n in Eq. (1), and so to apply Eq. (1), we need to derive a sound measurement for M_n based on the novel reflective measurement M_r that Wall-Street makes. As illustrated in Fig. 8, M_n is the signal strength between the neighboring gNB to UE through the surface (red dotted line). To infer M_n , Wall-Street uses the RSRP of a link between the source gNB and UE (M_s) and between the neighboring cell and the source gNB (M_r). We can simplify the link budget of each RSRP measurement as follows:

$$M_s = G_{gNB_s} + L_{gNB_s} + G_{w,tra} + G_{UE} + L_{UE} + L_{car} \quad (2)$$

$$M_n = G_{gNB_n} + L_{gNB_n} + G_{w,tra} + G_{UE} + L_{UE} + L_{car} \quad (3)$$

where G_{gNB_s} and G_{gNB_n} are the gain of the source and neighbor gNBs respectively, L_{gNB_s} and L_{gNB_n} are the free-space path loss between the source and neighbor gNBs and the surface, respectively, $G_{w,tra}$ is the transmission gain of the surface, G_{UE} is the gain of the UE, L_{UE} is the free-space path loss between the UE and the surface, and L_{car} is the loss from a car window. Likewise, we can calculate the signal strength measured by the source gNB (M_r) as:

$$M_r = G_{gNB_n} + L_{gNB_n} + G_{w,ref} + G_{gNB_s} + L_{gNB_s} + 2 \cdot L_{car} \quad (4)$$

where $G_{w,ref}$ is the reflection gain of the surface. Summing Eqs. (2) and (3), we calculate M_n as

$$M_n = M_r - M_s - G_{w,ref} + 2 \cdot (G_{w,tra} + G_{UE} + L_{UE}). \quad (5)$$

Practically, given the distance between Wall-Street and any gNB is significantly greater than the distance between UE and Wall-Street we can approximate the UE-to-surface distance as one meter with an approximate free space path loss, denoted L_{UE} . Since the source gNB controls the reflecting surface, it

has knowledge of the surface’s reflective gain $G_{w,ref}$ and transmissive gain $G_{w,tra}$. Also, as the gNB controls the transmit power of the UE in 3GPP,¹ it also knows the UE’s transmit gain G_{UE} . By utilizing this information, the source gNB can infer the RSRP between the target cell and the UE, enabling it to make effective handover decisions.

3.2.2 Handover Execution

The source gNB decides whether to initiate a handover using Eqs. (1) and (5), and upon proceeding, sends a HO Req message to the target gNB. Upon receiving the corresponding HO ACK, the source gNB then triggers Wall-Street to switch to downlink beam combining and uplink beam splitting, and sends a HO command to the UE. Instead of detaching from the source gNB, however, the UE synchronizes with the target gNB via the RACH, using the 3GPP-standardized Dual Active Protocol Stack (DAPS) [2], maintaining two active protocol stacks. Upon receiving the HO command, the UE suspends the source cell *Signaling Radio Bearers* (SRBs), which are in charge of control-plane signaling (including Wall-Street control), and establishes SRBs for the target cell. The UE receives user data simultaneously from both source and target cells (on different channels), and we reconfigure the Packet Data Convergence Protocol (PDCP) layer to a common PDCP entity for the source and target user plane protocol stacks.

When the UE moves at vehicular speed, packets are prone to loss especially at the moment of handover when signal strength is typically weakest. So to ensure reliable packet delivery, the source and target gNBs send duplicate data packets during handover execution, and the UE’s PDCP layer reorders and de-duplicates them. For packet flow in the uplink, the UE sends the same packet to the source and target gNB, which forwards the received ACK through the Xn link and dequeues the packet in the shared buffer. Wall-Street’s PHY configuration remains the same for both downlink and uplink as in the preparation phase.

Handover execution at the PHY: Upon receiving a handover execution trigger from the serving gNB, Wall-Street switches between beam combining for the downlink packet flow from two gNBs and beam splitting for the uplink packet flow to two gNBs. Wall-Street simultaneously steers the downlink combination and uplink split at the same angle due to angular reciprocity. Specifically, given a certain biasing voltage configuration applied to the surface that creates a transmissive combination of two different angles for downlink signals, uplink signals impinging on the surface will be redirected toward the same angles in the uplink. Hence, angular reciprocity facilitates fast beam alignments as the surface configuration optimized for downlink transmissions works under the uplink communication, and vice versa.

¹The gNB sends Downlink Control Information (DCI) to send power control commands to the UE.

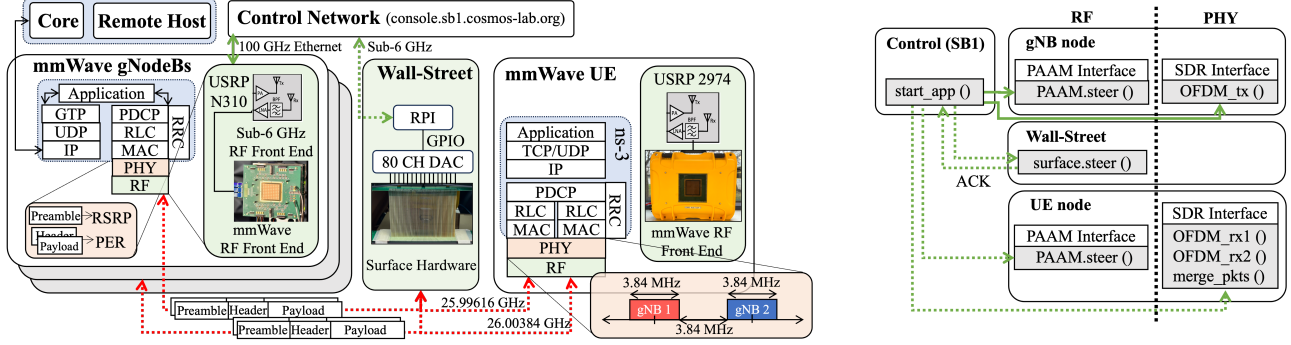


Figure 9— Wall-Street-COSMOS testbed integration: we integrate Wall-Street with COSMOS USRP-based gNBs and UE (left). We illustrate a simplified control flow of Wall-Street-integrated COSMOS testbed (right).

3.2.3 Handover Completion

When Eq. (1) holds true for a threshold *time-to-handover* duration, the target cell completes the handover by sending the source cell a UE release indication and triggering a signal to Wall-Street indicate handover is complete. If handover fails, the UE immediately reverts to the source cell configuration and re-activates source cell SRBs for control-plane signaling. This prevents the UE from disconnecting completely.

Handover completion at the PHY: When the source gNB triggers a signal to complete handover, the surface maximizes the power of the transmission link with the new cell by reverting to a single beam mode. If the handover fails, instead maximizes the power of the link with the old cell, maintaining the connection and preventing service disruption for the UE.

3.2.4 Multi-user Support

When a handover is executed for a UE in a vehicle, other UEs sharing the same Wall-Street within that vehicle do not need to undergo a separate handover procedure. Instead, the HO Request encapsulates the contexts of all UEs associated with each Wall-Street, allowing all UEs to be handed over simultaneously using the procedure above.

4 Implementation

We illustrate our Wall-Street implementation in Fig. 9. It consists of: (1) a surface hardware and control unit; (2) integration with the COSMOS testbed, implementing new PHY features; and (3) an ns-3 simulation for evaluating TCP end-to-end performance, using a state-of-the-art mmWave ns-3 simulator [18] with our own modifications, in SA mode. The simulation is trace-driven, fed with PHY traces collected from real-time experiments in the Wall-Street-integrated testbed.

4.1 Wall-Street Hardware

The Huygens metasurface (HMS) is a metamaterial smart surface that reflects and refracts mmWave signals, and that

prior work has demonstrated at 24 GHz [6]. Wall-Street for the first time demonstrates an HMS at 26 GHz. The Wall-Street surface is composed of 76 boards, each consisting of 28 co-located magnetic and electric unit cells. A control unit connected to Wall-Street supplies a set of voltages to the boards, and the beam is collectively shaped by all boards forming an array factor. Two 40-channel AD5370 16-bit DACs provide independent control of the unit cells on each Wall-Street board, with each channel supplying a variable 0 to 16 V control voltage. To expedite the steering process, one channel supplies the voltage to two adjacent boards, enabling two DACs to independently control all boards, representing a savings of control logic relative to prior work [6]. The two DACs are each connected to the Serial Peripheral Interface (SPI) of a Raspberry Pi (RPI) through GPIO. The RPI listens for control signals from the COSMOS testbed control network, known as sandbox1 (SB1), via sub-6 GHz. Upon receiving a signal, it sends a command to the DACs, which then apply the appropriate voltage levels. These voltage levels are determined from a pre-stored voltage-to-phase look-up table. The steering speed of the Wall-Street hardware has been optimized to 0.2 ms for real-time implementation.

4.2 COSMOS Testbed

The COSMOS testbed comprises mmWave software-defined radios (SDRs) integrated with the IBM mmWave Phased-Array Antenna Module (PAAM) frontends (Fig. 9) and USRPs [10]. The PAAM features 4 tiled RFICs, each with 32 TRx phase-shifting elements, supporting a total of 64 antennas. It enables hybrid analog-digital beamforming with up to 8 independent beams, a 30-degree steerable beamwidth, and 43 dBm EIRP. The PAAM offers full access to beamforming control and latency as low as 10s of nanoseconds for low-latency MAC and hybrid beamforming. Stationary PAAM devices are used as gNBs, as shown in Fig. 10(a), with their IF ports connected to the RF ports of a USRP N310 for baseband signal processing. These stationary PAAMs are mounted on a remotely controllable XY table and connected to the SB1 through Ethernet, enabling control over the network. For the

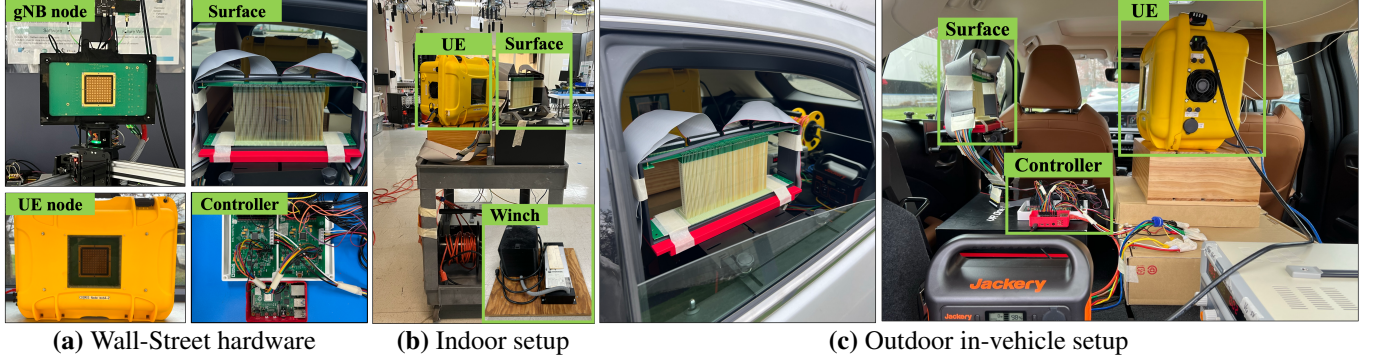


Figure 10— Wall-Street’s hardware implementation and testbed: showing (a) individual hardware components, (b) indoor experimental UE-side setup, and (c) outdoor in-vehicle UE-side configuration.

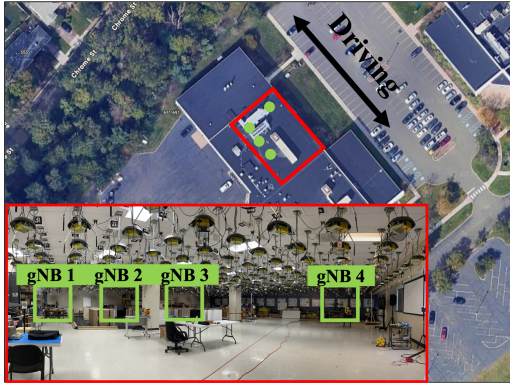


Figure 11— Experimental gNB-side testbed setup and map: we deploy four gNBs on the first floor of a lab facing an outdoor parking lot. The vehicle is ≥ 30 m. from the gNBs.

UE, a portable PAAM device is employed, as depicted in Fig. 10(a), utilizing the USRP 2974 for baseband processing and front-end control.

4.2.1 PHY implementation on COSMOS

We developed new features on the PHY layer of the COSMOS testbed, including OFDM packet transmission and reception at one or more channels, extraction of RSRP and Packet Error Rate (PER) from the packet, and IBM PAAM and Wall-Street beam control. Periodic bursts of OFDM packets are sent from two PAAMs in different frequency bands with 3.84 MHz separation, and the receiver simultaneously decodes packets from both transmitters by operating at a larger bandwidth. Specifically, the receiver extracts RSRP from the reference signal in the preamble, the packet sequence number from the header, and the PER from the cyclic redundancy check (CRC). During handover, the source and target gNBs transmit identical packets. Wall-Street combines the downlink channels, enabling the UE to decode packets on both channels simultaneously and compute the combined PER. A C++ script in SB1 sends control commands to the gNB and Wall-Street to follow the procedure, as illustrated in Fig. 9 (right).

5 Evaluation

We first conduct field studies to evaluate the end-to-end performance of Wall-Street and compare it with a 3GPP standardized 5G SA handover protocol (§5.2). We then present micro-benchmark experiments to provide further insight into which factors impact Wall-Street’s performance (§5.3).

5.1 Methodology

We conduct evaluations of various indoor and outdoor driving scenarios with four gNBs and one UE. For indoor settings, we place the nodes in a lab measuring 20×30 m, as shown in Fig. 10(b). To test the UE and Wall-Street under mobility, we place them on a cart, connected to a cable on the winch that pulls the cart in a constant speed of approximately 1 km/h. For outdoor settings, we mount the surface on the rear window and deploy the UE node on the opposite side of the rear seat in a SUV vehicle, driving at different speed, ranging from 5 to 15 km/h. The location of the UE in the vehicle is the same for the baseline. Both surface and UE are powered with a portable battery. Due to fixed gNB locations, we were able to drive up to 40 m on the trajectory shown in Fig. 11 for outdoor scenarios and 20 m for the indoor scenario.

We implement the 5G SA HO protocol described in §2 and deploy it on our testbed for comparison. We term this scheme as the baseline, using it as a performance benchmark in the remainder of our evaluation. For both Wall-Street and baseline, the hysteresis parameter H of A3 event in Eq. (1) is set to 10 dB with TTT of 150 ms and the measurement report periodicity of 160 ms. For the baseline, a total duration of every measurement report takes less than 20 ms with three neighbor gNBs. We set our time-to-handover to 300 ms.

5.2 End-to-end Throughput and Delay

We evaluate end-to-end performance of Wall-Street delivering bulk TCP data flows. To quantify performance, we calculate throughput as the total data bits divided by the duration, measured every 100 ms. We average the round-trip-time (RTT)

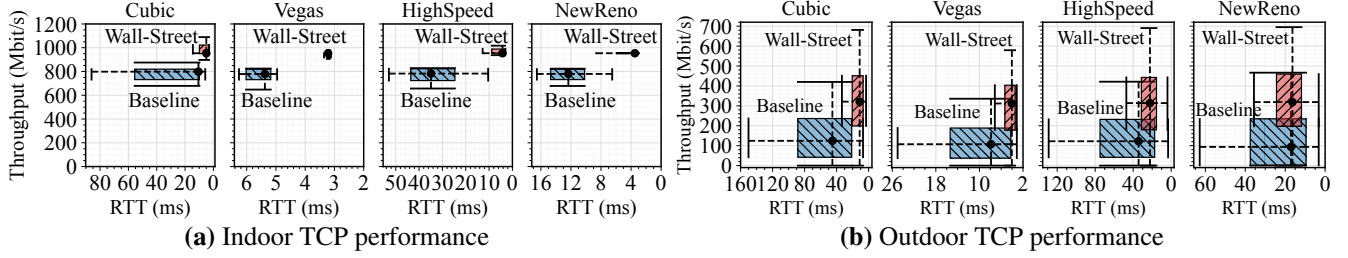


Figure 12— Throughput and round trip time (RTT) achieved by four congestion control algorithms. The right and lower edge of the box represents the 25% percentile, respectively. The left and upper edge give the 75th percentiles. The two ends of the error bar gives the 10th and 90th percentiles. The intersection point of the horizontal and vertical error bar represents the median value.

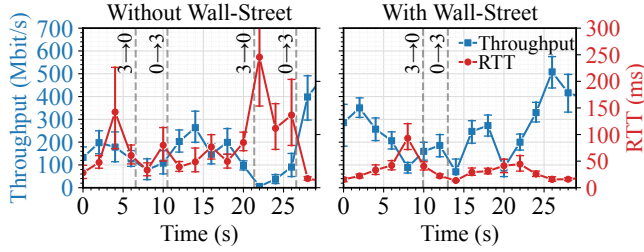


Figure 13— Throughput and delay achieved without Wall-Street (*left*) and with Wall-Street (*right*) as the vehicle is moving along the same trajectory. Vertical dashed lines indicate the handover event.

of packets over every 100 ms.

TCP performance under various settings. We evaluate the throughput and RTT of Wall-Street and the baseline under indoor and outdoor settings using four congestion control algorithms: CUBIC, Vegas, HighSpeed, and NewReno. In the indoor scenario shown in Fig. 12(a), Wall-Street increases the average throughput by at least $\times 1.2$ and decreases the delay by $\times 0.4$ - 0.8 compared to the baseline. In the outdoor scenario shown in Fig. 12(b), Wall-Street improves the throughput by $\times 2.5$ - 3.4 and decreases the delay by $\times 0.4$ on average. The delay variance of the baseline is typically higher than the variance of Wall-Street for both indoor and outdoor scenario. We note that mmWave signals in the outdoor testbed fluctuate significantly due to vehicle speed and car-body blockages, and signal strengths are weaker than indoors due to larger link distances. This leads to more frequent outages and handovers as well as a higher likelihood of incorrect handover decisions, which impacts overall performance, yet provides Wall-Street with more room for improvement. In the following, we present factors that impact Wall-Street’s performance.

TCP performance over time. To further demonstrate Wall-Street’s performance, we divide the 30-second outdoor experiment into 15 equal intervals of two seconds each. We then plot the median throughput and delay for each interval, comparing Wall-Street with the baseline in Fig. 13. Handover events are indicated by vertical dashed lines. Throughout the entire experiment, Wall-Street consistently achieves higher throughput than the baseline. This is because Wall-Street does not stop data exchange for the measurement report, ensuring

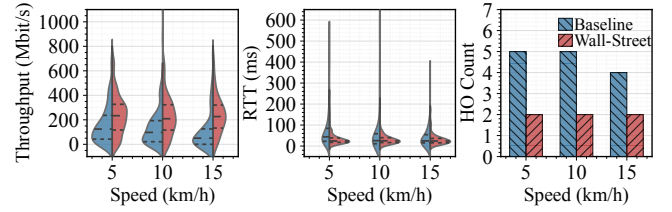


Figure 14— Impact of speed: throughput, RTT, HO count (*left to right*) with different speed, ranging from 5 km/h to 15 km/h.

a seamless flow of data. Moreover, Wall-Street exhibits lower latency with fewer handover ping-pongs. While the baseline experiences an outage at the 21 s mark immediately after the handover, Wall-Street maintains a stable connection without any outages. This is attributed to Wall-Street’s robust handover mechanism where the handover is only completed when the A3 event remains true for a predefined threshold duration. This approach enhances the reliability of the handover process, reducing the chance of a wrong handover choice.

Impact of vehicle speed. Figure 14 presents an analysis of Wall-Street’s performance at various driving speeds, ranging from 5 km/h to 15 km/h. The throughput, RTT, and handover count of Wall-Street are compared against the baseline. Across all driving scenarios, Wall-Street demonstrates better performance, with higher throughput, lower latency, and fewer handover triggers than the baseline. Notably, while increasing the speed of the vehicle adversely affects the throughput of the baseline, Wall-Street’s average throughput remains relatively unaffected by the change in speed. This highlights Wall-Street’s robustness and ability to maintain stable performance even under varying mobility conditions.

Impact of handover preparation. Figure 15 (*left*) illustrates the increase in sequence numbers throughout the entire 30-second outdoor experiment, and Fig. 15 (*right*) shows the sequence number increase during the handover preparation phase. To better visualize the trend over time, a modulo operation is applied to the sequence numbers. The sequence numbers for Wall-Street increase rapidly over time compared to the baseline, indicating that more packets are successfully delivered. During the handover preparation phase, the baseline’s sequence number does not increase periodically, result-

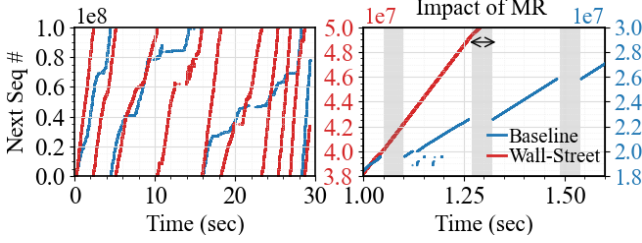


Figure 15— Measurement report impact: increase trend of sequence numbers during the entire 30s experiment (*left*) and handover preparation (*right*).

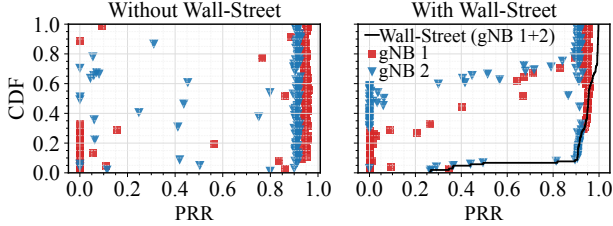


Figure 16— Make-before-break impact: packet reception rate of a link from each gNB without Wall-Street (*left*) and that of each gNB and of two links (packet duplication) from two gNB with Wall-Street along the same trajectory (*right*).

ing in a lower slope of the trend. This is because the UE stops communicating with the source gNB and listens for the SSB burst from neighboring gNBs. It is important to note that while measuring all neighboring gNBs takes less than 20 ms, the impact of this process lasts for 50 ms, causing a significant disruption in the baseline’s packet delivery. In contrast, Wall-Street maintains a consistent increase in sequence numbers during the handover preparation phase.

Impact of make-before-break handover. We present the cumulative distribution function (CDF) of the packet reception rate (PRR) during soft handover. PRR values are extracted from the UE by decoding the CRC for every 2000 packets. PRRs at a given timestamp are plotted on the same y-axis value for both subplots in Fig. 16. A black line represents Wall-Street’s combined PRR with packet duplication from gNB 1 and 2. Markers on Fig. 16 (left) are PRRs from each link without Wall-Street, while markers on Fig. 16 (right) denote PRRs from a link through Wall-Street but without packet duplication. With Wall-Street, each link in fact has lower PRR compared to the baseline. This is because when Wall-Street establishes beam combining, it divides the power across two links, resulting in weaker signal strength for each link compared to the baseline. However, by combining the beams and sending duplicate packets, Wall-Street guarantees a PRR greater than 90% for 92% of the handover execution times and eliminates instances of packet error. In contrast, each link suffers from low PRR with the baseline, leading to potential packet loss and degraded performance. This result implies that at the moment of handover when signals are weak, make-before-break enhances the handover reliability.

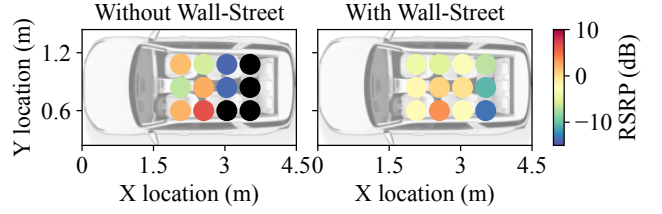


Figure 17— In-vehicle mmWave coverage. ●: no signal.

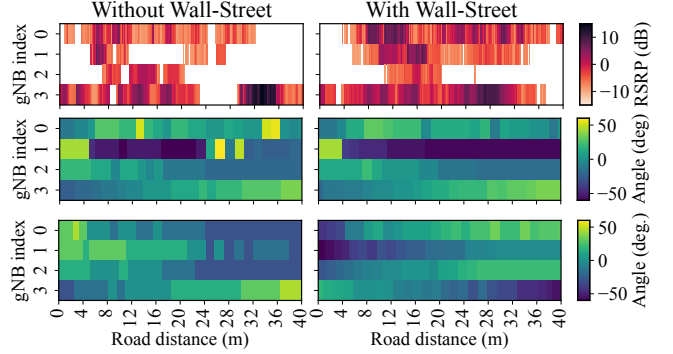


Figure 18— RSRP heatmap (upper) and corresponding gNB beam angles (middle) and UE/surface angles (lower) heatmaps (left: without Wall-Street; right: with Wall-Street and UE beam fixed to the surface). In-vehicle location of the UE is the same in both scenarios.

5.3 Microbenchmarks

We evaluate Wall-Street’s in-vehicle signal coverage, multi-beam operations at the physical layer, far-field beam pattern measured with the spectrum analyzer, and near-field measurements using the vector network analyzer (VNA) at 26 GHz.

In-vehicle mmWave coverage. To evaluate Wall-Street’s signal coverage enhancement, we mount the surface on the rear window. The gNB, located 40 meters away from the vehicle, transmits signals towards the window. We then move the UE to various locations inside the vehicle and measure the maximum RSRP during an exhaustive search between the gNB’s beam angle and UE or surface’s steering angle. With Wall-Street, we steer the UE’s receiving beam towards the surface. Fig. 17 shows that while the UE located in the backseats experiences signal outage with the baseline setup, Wall-Street guarantees an outage-free experience at all locations within the vehicle. Moreover, Wall-Street provides more than 12 dB gain at various in-vehicle locations.

Beam tracking under mobility. Figure 18 (upper) shows the RSRP heatmap of the road shown in Fig. 11 as the vehicle moves. Two bottom subplots show the corresponding gNB beam angle distribution and UE/surface angle distribution, respectively. With Wall-Street, the UE angle is fixed towards the surface. We see that the gNB angle distributions are similar with and without Wall-Street, and the UE/surface angle distribution are nearly complementary. Without Wall-Street,

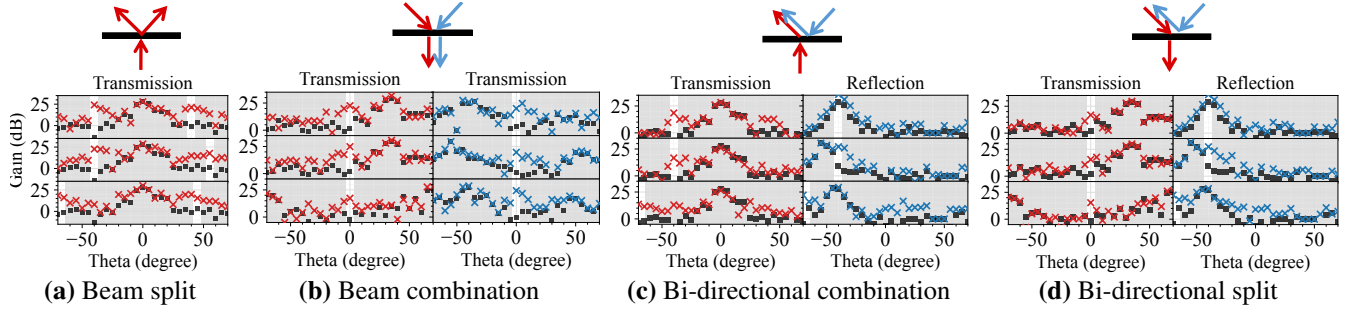


Figure 19— Wall-Street’s beam patterns over four operations. \times : empirical spectrum analyzer data; \blacksquare : benchmark data with the surface is set to 0V. The steering angles are highlighted in the background. 0 dB represents the spectrum analyzer noise floor (*upper*: $-40^\circ/40^\circ$; *middle*: $-40^\circ/55^\circ$; *lower*: $-68^\circ/45^\circ$). Red and blue markers are measured at 26 GHz and 26.1 GHz, respectively.

the signals suddenly disappear along the road, especially for gNB 1, due to a car-body blockage.

Multi-link operations. We evaluate Wall-Street’s capability to manipulate multiple beams at various indoor locations. Fig. 20(a) presents the RSRP heatmap without Wall-Street, with the upper heatmaps showing RSRPs when each gNB and UE beams are aligned, and the lower heatmaps showing RSRPs when each gNB steers its beam towards the UE, but the UE fixes its angle at 0° . Fig. 20(b) shows the heatmaps with Wall-Street during the measurement report process (*upper*) and make-before-break handover execution (*lower*). The upper left subplot evaluates the RSRP from gNB 0, and the upper right subplot shows the RSRP from gNB 1. Overall, the signal strength is significantly greater than Fig. 20(a) (*lower*) and slightly less than in Fig. 20(a) (*upper*), which is expected due to power splitting. The lower subplot on Fig. 20(b) presents the inferred RSRP from packets received at gNB 0 (*left*) and gNB 1 (*right*) when Wall-Street reflects signals from another gNB and refracts signals from the UE. Both heatmaps demonstrate that signals reflected by Wall-Street can be accurately inferred, as described in §3.2.1.

Far-field beam patterns. Figure 19 presents beam patterns for Wall-Street’s four operation modes: beam split, single-directional beam combination, bi-directional beam combination and bi-directional beam splitting. We choose four sets of beam angles ($-40^\circ/40^\circ$, $-40^\circ/55^\circ$, and $-68^\circ/45^\circ$), the angle near the intersection of two gNBs’ coverage areas. To measure the beam pattern, we place the transmit and receive horn antennas two meters away from Wall-Street and record the gain of Wall-Street as we move the receiver from -70° to 70° with respect to Wall-Street. Since we did not use an anechoic chamber, the beam passes around the surface. To accurately capture the beam pattern, we also measure the beam pattern when Wall-Street is set to 0V, hence not steering the incident beam. We use these measurements as a benchmark and denote them with \blacksquare . We set 0 dB as a noise floor of the spectrum analyzer and correspondingly scale the results. Since Wall-Street operates at two different channels, a transmitter on left (red arrows) and transmitter on right (blue arrows)

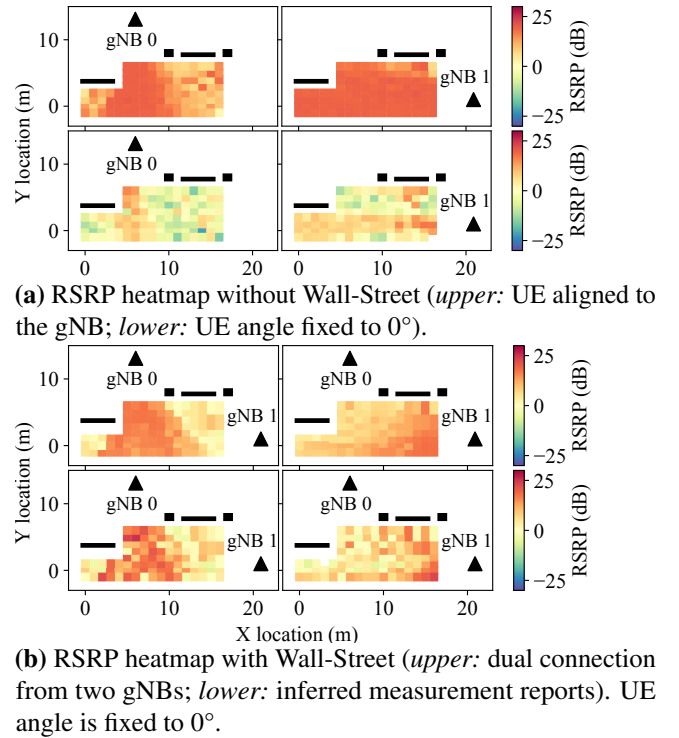


Figure 20— Multi-link operations. We use the following notations: gNB \blacktriangle , UE \square , blockage \blacksquare .

transmit signals at 26 GHz and 26.1 GHz, respectively. Compared to the benchmark, we observe nearly 20 to 25 dB gain in each direction except when a steered beam aligns with the specular reflection of the transmitter (e.g., $-40^\circ/40^\circ$ reflection in Fig. 19(c) and Fig. 19(d)). Also, we observe that when the beam is steered into a wider angle, the gain drops. The voltage configurations of Figs. 19(a) and 19(b) are identical, demonstrating that angular reciprocity holds even under multi-beam operation and enabling fast switching of uplink/downlink packet flow during handover.

Beam power ratio. Figure 21 compares beam patterns with different power ratios: 0.5/0.5 and 0.75/0.25 split. For all three multi-beam operations, the gain of the beam on left

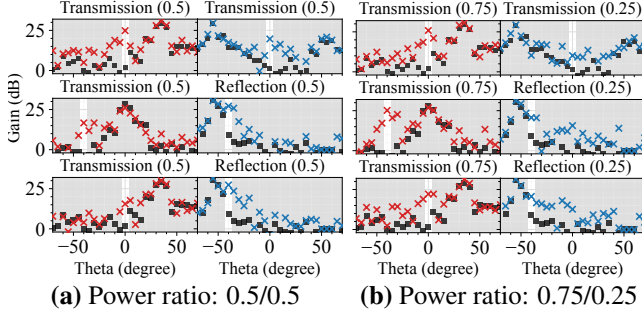


Figure 21— Power ratio adjustment with the steering angle of $-40^\circ/55^\circ$ (*upper*: beam combination; *middle*: bi-directional combination; *lower*: bi-directional split).

(denoted with red markers) increases while the gain of the beam on right (denoted with blue markers) decreases as we shift the ratio from 0.5/0.5 to 0.75/0.25, demonstrating Wall-Street’s capability to flexibly adjust the power ratio between two beams.

Near-field huygens pattern Figure 22 shows the near-field VNA measurement on Wall-Street at 26 GHz. By adjusting the voltage applied to both the magnetic (U_M) and electric (U_E) unit cells, the surface achieves 2π phase coverage with near-unity magnitude for both reflection and transmission.

6 Related Work

Prior electronically-tunable mmWave and THz surface designs steer a single link at the physical layer using various techniques: relay switches and phase delay lines controlling patch antennas in a reflective configuration [27], PIN diodes controlling patch antennas in a reflective configuration [8, 9, 32], varactor diodes controlling patch antennas in a reflective configuration [30], or varactor diodes controlling split ring resonators in a Huygens reflective-transmissive configuration [6]. Other designs take an actively-amplified, amplify-and-forward approach at the physical layer [4]. Some THz designs are similar in concept yet differ in substrate, leveraging switched 65 nm CMOS process controlling ring resonators for a 0.3 THz design [29]. However, these proposals stop short of co-designing the surface’s involvement with 5G’s handover protocol and RAN architecture as Wall-Street does. NR-Surface [15] is a 24 GHz, varactor-controlled patch antenna reflective surface that integrates with 5G New Radio’s beam management, but does not offer a transmissive mode as Wall-Street does, for the common case where the client and cell are on opposite sides of the surface. Further, our experimental evaluation probes end-to-end, transport-layer performance, going beyond NR-Surface’s strictly physical-layer measurement results.

Prior passive/static mmWave reflector designs leverage electronic beam steering capabilities of base stations and clients with typically larger surfaces that reflect in many different directions. At 60 GHz, MilliMirror [22] proposes a novel,

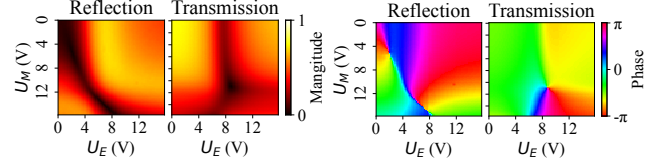


Figure 22— Wall-Street’s VNA measurement response: we show reflection (*left* sub-plots) and transmission through the surface (*right* sub-plots).

3D-printed surface synthesis algorithm. However, similarly to prior electronically-tunable surface work, these systems also stop short of 5G RAN co-design.

Prior roadside/trackside handover designs Polycorn [21] and Wi-Fi Goes to Town [26] orchestrate packet flow for (low band) LTE and Wi-Fi trackside and roadside networks, respectively, transferring packets from one cell or access point in the radio access network in order to best serve highly-mobile users. Wall-Street, in contrast, leverages the unique capabilities of smart surfaces and (high band) mmWave communications to split and combine beams to and from roadside mmWave cells in a way these prior designs do not anticipate. REM [16] uses Orthogonal Time Frequency Modulation in the LTE low band (sub-6 GHz) to simplify the conventional low-band signal strength based handover sequence, but does not target the larger frequency bandwidths and smaller cell sizes of mmWave 5G NR.

Work in mmWave beam alignment maintains a connection once it has been established via beam search. Representative works include Agile-Link [12], which proposes multi-armed beams and a postprocessing algorithm to accelerate the alignment time to be logarithmic in the number of possible beam directions. LiSteer [10] uses mmWave access point indicator LEDs and an array of mobile client-mounted light sensors to infer client bearing to the access point. BounceNet [14] proposes an architecture and algorithm for aligning many walking speed clients’ 802.11ad links with many nearby 60 GHz access points, in a relatively dense access point deployment scenario, targeting a different problem than Wall-Street.

7 Conclusion

This paper introduces Wall-Street, the first smart surface-enabled 5G mmWave roadside networking solution designed to efficiently steer outdoor mmWave signals into vehicles, enable simultaneous data exchange and neighboring cell measurements, and facilitate seamless and reliable handovers through a make-before-break process. We conduct an extensive evaluation in various indoor and outdoor settings, demonstrating significant TCP improvement. We believe Wall-Street is the first step in scaling out the capacity of mmWave networks and paves the way for future advancements in mmWave communications, particularly in vehicular networks.

8 Acknowledgements

This material is based upon work supported by the National Science Foundation under Grants No. CNS-2148271 and CNS-2232459, and is supported in part by funds from federal agency and industry partners as specified in the Resilient & Intelligent NextG Systems (RINGS) program. We gratefully acknowledge the support of a grant from the Princeton University School of Engineering and Applied Science Innovation Fund.

References

- [1] 3GPP. Study on new radio access technology physical layer aspects. Technical Report (TR) 38.802, 3rd Generation Partnership Project (3GPP), 2017.
- [2] 3GPP. 5G; NR; NR and NG-RAN Overall description; Stage-2. Technical Report (TR) 38.300, 3rd Generation Partnership Project (3GPP), 2021.
- [3] 3GPP. Release 17 Description; Summary of Rel-17 Work Items. Technical Report (TR) 21.917, 3rd Generation Partnership Project (3GPP), 2022.
- [4] O. Abari, D. Bharadia, A. Duffield, D. Katabi. Enabling High-Quality Untethered Virtual Reality. *14th USENIX Symposium on Networked Systems Design and Implementation (NSDI)*, 531–544, 2017. ISBN 978-1-931971-37-9.
- [5] Y. Azar, G. N. Wong, K. Wang, R. Mayzus, J. K. Schulz, H. Zhao, F. Gutierrez, D. Hwang, T. S. Rappaport. 28 GHz propagation measurements for outdoor cellular communications using steerable beam antennas in New York city. *IEEE International Conference on Communications (ICC)*, 5143–5147, 2013. doi:10.1109/ICC.2013.6655399. ISSN: 1938-1883.
- [6] K. W. Cho, M. H. Mazaheri, J. Gummesson, O. Abari, K. Jamieson. mmWall: A Steerable, Transflective Metamaterial Surface for NextG mmWave Networks. *20th USENIX Symposium on Networked Systems Design and Implementation (NSDI)*, 1647–1665, 2023. ISBN 978-1-939133-33-5.
- [7] H. Deng, C. Peng, A. Fida, J. Meng, Y. C. Hu. Mobility Support in Cellular Networks: A Measurement Study on Its Configurations and Implications. *Proceedings of the Internet Measurement Conference 2018*, 147–160. ACM, Boston MA USA, 2018. ISBN 978-1-4503-5619-0. doi:10.1145/3278532.3278546.
- [8] J.-B. Gros, V. Popov, M. A. Odit, V. Lenets, G. Lerosey. A Reconfigurable Intelligent Surface at mmWave Based on a Binary Phase Tunable Metasurface. *IEEE Open Journal of the Communications Society*, 2, 1055–1064, 2021. ISSN 2644-125X. doi:10.1109/OJCOMS.2021.3076271.
- [9] J.-B. Gros, L. Santamaria, V. Popov, M. Odit, V. Lenets, X. Lleshi, A. Toubal, Y. Nasser. Design of Reconfigurable Intelligent Surfaces at mmWave with Application to 5G/6G. *2023 17th European Conference on Antennas and Propagation (EuCAP)*, 1–4. IEEE, Florence, Italy, 2023. doi:10.23919/EuCAP57121.2023.10133769.
- [10] M. K. Haider, Y. Ghasempour, D. Koutsonikolas, E. W. Knightly. LiSteer: mmWave Beam Acquisition and Steering by Tracking Indicator LEDs on Wireless APs. *Proceedings of the 24th Annual International Conference on Mobile Computing and Networking (MobiCom)*, 273–288. ACM, New Delhi India, 2018. ISBN 978-1-4503-5903-0. doi:10.1145/3241539.3241542.
- [11] A. Hassan, A. Narayanan, A. Zhang, W. Ye, R. Zhu, S. Jin, J. Carpenter, Z. M. Mao, F. Qian, Z.-L. Zhang. Vivisecting mobility management in 5G cellular networks. *Proceedings of the ACM SIGCOMM 2022 Conference, SIGCOMM '22*, 86–100. Association for Computing Machinery, New York, NY, USA, 2022. ISBN 9781450394208. doi:10.1145/3544216.3544217.
- [12] H. Hassanieh, O. Abari, M. Rodriguez, M. Abdelghany, D. Katabi, P. Indyk. Fast millimeter wave beam alignment. *Proceedings of the Conference of the ACM Special Interest Group on Data Communication (SIGCOMM)*, 432–445. ACM, Budapest Hungary, 2018. ISBN 978-1-4503-5567-4. doi:10.1145/3230543.3230581.
- [13] I. A. Hemadeh, K. Satyanarayana, M. El-Hajjar, L. Hanzo. Millimeter-Wave Communications: Physical Channel Models, Design Considerations, Antenna Constructions, and Link-Budget. *IEEE Communications Surveys & Tutorials*, 20(2), 870–913, 2018. ISSN 1553-877X, 2373-745X. doi:10.1109/COMST.2017.2783541.
- [14] S. Jog, J. Wang, J. Guan, T. Moon, H. Hassanieh, R. R. Choudhury. Many-to-Many Beam Alignment in Millimeter Wave Networks. *USENIX Symposium on Networked Systems Design and Implementation (NSDI)*, 2019. ISBN 978-1-931971-49-2.
- [15] M. Kim, N. Ahn, S. M. Kim. NR-Surface: NextG-ready μ W-reconfigurable mmWave Metasurface. *USENIX Symposium on Networked Systems Design and Implementation (NSDI)*, 2024. ISBN 978-1-939133-39-7.
- [16] Y. Li, Q. Li, Z. Zhang, G. Baig, L. Qiu, S. Lu. Beyond 5G: Reliable Extreme Mobility Management. *Proceedings of the Annual conference of the ACM Special Interest Group on Data Communication on the applications, technologies, architectures, and protocols for computer communication*, 344–358. ACM, Virtual Event USA, 2020. ISBN 978-1-4503-7955-7. doi:10.1145/3387514.3405873.
- [17] G. R. MacCartney, T. S. Rappaport, S. Rangan. Rapid Fading Due to Human Blockage in Pedestrian Crowds at 5G Millimeter-Wave Frequencies. *IEEE Global Communications Conference, GLOBECOM*, 1–7. IEEE, Singapore, 2017. ISBN 978-1-5090-5019-2. doi:10.1109/GLOCOM.2017.8254900.
- [18] M. Mezzavilla, M. Zhang, M. Polese, R. Ford, S. Dutta, S. Rangan, M. Zorzi. End-to-End Simulation of 5G mmWave Networks. *IEEE Communications Surveys & Tutorials*, 20(3), 2237–2263, 2018. ISSN 1553-877X. doi:10.1109/COMST.2018.2828880.
- [19] A. Narayanan, E. Ramadan, J. Carpenter, Q. Liu, Y. Liu, F. Qian, Z.-L. Zhang. A First Look at Commercial 5G Performance on Smartphones. *Proceedings of The Web Conference (WWW)*, 894–905. ACM, Taipei Taiwan, 2020. ISBN 978-1-4503-7023-3. doi:10.1145/3366423.

- 3380169.
- [20] A. Narayanan, X. Zhang, R. Zhu, A. Hassan, S. Jin, X. Zhu, X. Zhang, D. Rybkin, Z. Yang, Z. M. Mao, F. Qian, Z.-L. Zhang. A variegated look at 5G in the wild: performance, power, and QoE implications. *Proceedings of the Conference of the ACM Special Interest Group on Data Communication (SIGCOMM)*, 610–625. ACM, New York, NY, USA, 2021. ISBN 978-1-4503-8383-7. doi:10.1145/3452296.3472923.
 - [21] Y. Ni, F. Qian, T. Liu, Y. Cheng, Z. Ma, J. Wang, Z. Wang, G. Huang, X. Liu, C. Xu. POLYCORN: Data-driven Cross-layer Multipath Networking for High-speed Railway through Composable Schedulerlets. *20th USENIX Symposium on Networked Systems Design and Implementation (USENIX NSDI)*, 1325–1340, 2023. ISBN 978-1-939133-33-5.
 - [22] K. Qian, L. Yao, X. Zhang, T. N. Ng. MilliMirror: 3D printed reflecting surface for millimeter-wave coverage expansion. *Proceedings of the 28th Annual International Conference on Mobile Computing And Networking (MobiCom)*, 15–28. ACM, Sydney NSW Australia, 2022. ISBN 978-1-4503-9181-8. doi:10.1145/3495243.3517024.
 - [23] S. Rangan, T. S. Rappaport, E. Erkip. Millimeter-Wave Cellular Wireless Networks: Potentials and Challenges. *Proceedings of the IEEE*, **102**(3), 366–385, 2014. ISSN 1558-2256. doi:10.1109/JPROC.2014.2299397.
 - [24] T. S. Rappaport, G. R. MacCartney, S. Sun, H. Yan, S. Deng. Small-Scale, Local Area, and Transitional Millimeter Wave Propagation for 5G Communications. *IEEE Transactions on Antennas and Propagation*, **65**(12), 6474–6490, 2017. ISSN 0018-926X, 1558-2221. doi:10.1109/TAP.2017.2734159.
 - [25] D. Raychaudhuri, I. Seskar, G. Zussman, T. Korakis, D. Kilper, T. Chen, J. Kolodziejski, M. Sherman, Z. Kostic, X. Gu, H. Krishnaswamy, S. Maheshwari, P. Skrimponis, C. Gutterman. Challenge: COSMOS: A city-scale programmable testbed for experimentation with advanced wireless. *Proceedings of the 26th Annual International Conference on Mobile Computing and Networking, MobiCom '20*, 1–13. Association for Computing Machinery, New York, NY, USA, 2020. ISBN 978-1-4503-7085-1. doi:10.1145/3372224.3380891.
 - [26] Z. Song, L. Shangguan, K. Jamieson. Wi-Fi Goes to Town: Rapid Picocell Switching for Wireless Transit Networks. *Proceedings of the Conference of the ACM Special Interest Group on Data Communication (SIGCOMM)*, 322–334. ACM, New York, NY, USA, 2017. ISBN 978-1-4503-4653-5. doi:10.1145/3098822.3098846.
 - [27] X. Tan, Z. Sun, D. Koutsonikolas, J. M. Jornet. Enabling Indoor Mobile Millimeter-wave Networks Based on Smart Reflect-arrays. *IEEE Conference on Computer Communications (INFOCOM)*, 270–278. IEEE, Honolulu, HI, 2018. ISBN 978-1-5386-4128-6. doi:10.1109/INFOCOM.2018.8485924.
 - [28] A. Tassi, M. Egan, R. J. Piechocki, A. Nix. Modeling and Design of Millimeter-Wave Networks for Highway Vehicular Communication. *IEEE Transactions on Vehicular Technology*, **66**(12), 10,676–10,691, 2017. ISSN 0018-9545, 1939-9359. doi:10.1109/TVT.2017.2734684.
 - [29] S. Venkatesh, X. Lu, H. Saeidi, K. Sengupta. A high-speed programmable and scalable terahertz holographic metasurface based on tiled CMOS chips. *Nature Electronics*, **3**(12), 785–793, 2020. ISSN 2520-1131. doi:10.1038/s41928-020-00497-2.
 - [30] A. Wolff, L. Franke, S. Klingel, J. Krieger, L. Mueller, R. Stemler, M. Rahm. Continuous beam steering with a varactor-based reconfigurable intelligent surface in the Ka-band at 31 GHz. *Journal of Applied Physics*, **134**(11), 114,502, 2023. ISSN 0021-8979. doi:10.1063/5.0168330.
 - [31] D. Xu, A. Zhou, X. Zhang, G. Wang, X. Liu, C. An, Y. Shi, L. Liu, H. Ma. Understanding Operational 5G: A First Measurement Study on Its Coverage, Performance and Energy Consumption. *Proceedings of the Conference of the ACM Special Interest Group on Data Communication (SIGCOMM)*, 479–494. ACM, New York, NY, USA, 2020. ISBN 978-1-4503-7955-7. doi:10.1145/3387514.3405882.
 - [32] F. Yang, F. Xu, C. Liu, X. Yang, Z. Wang, J. Wu, X. Fu. Two-Dimensional Beam Steering Based on Compact Programmable Coding Metasurface. *Applied Sciences*, **12**(22), 11,780, 2022. ISSN 2076-3417. doi:10.3390/app122211780.
 - [33] H. Zhao, R. Mayzus, S. Sun, M. Samimi, J. K. Schulz, Y. Azar, K. Wang, G. N. Wong, F. Gutierrez, T. S. Rappaport. 28 GHz millimeter wave cellular communication measurements for reflection and penetration loss in and around buildings in New York city. *IEEE International Conference on Communications (ICC)*, 5163–5167, 2013. doi:10.1109/ICC.2013.6655403. ISSN: 1938-1883.